Lateral Boundary Conditions for Tropical Cyclone Models

JAMES J. HACK AND WAYNE H. SCHUBERT

Department of Atmospheric Science, Colorado State University, Fort Collins 80523

(Manuscript received 20 April 1980, in final form 3 March 1981)

ABSTRACT

Under certain circumstances a large fraction of the energy generated by the release of latent heat in a tropical cyclone can be partitioned to gravity-inertia wave motion rather than to balanced flow. In this way most of the generated energy is radiated away to the far field. If a primitive equation tropical cyclone model is to successfully simulate this process, its lateral boundary condition must be able to transmit the gravity-inertia wave energy generated in the interior of the model. Most present models seem deficient in this regard. As an improvement we explore the possibility of using a cylindrical, pure gravity wave radiation condition. Since there is a wide range of gravity wave phase velocities in a stratified atmosphere, it is necessary to apply the radiation condition vertical mode by vertical mode rather than level by level. The usefulness of this radiation condition and several other conditions in present use is tested both by a reflectivity analysis and by simple numerical time integrations.

1. Introduction

Numerical simulations of tropical cyclones are invariably attempted using models of limited horizontal extent, making the task of formulating an appropriate set of lateral boundary conditions unavoidable. The presence of a lateral boundary to the computational domains of these models is an artificial construct mandated only by the limitations of the computer. Thus, it is important that one seek a condition which minimizes the impact of this artificial boundary on the dynamical behavior of the phenomena being simulated inside it.

In a tropical cyclone, the large amount of latent heat released in deep convection continually disrupts any approximate balance of the mass and wind fields. The way in which the atmosphere responds to this heating (through the process of geostrophic or gradient adjustment) provides a basis for attaching importance to the formulation of lateral boundary conditions in tropical cyclone models. When latent heat is released on time scales shorter than the local adjustment time scale, and on horizontal scales typical of a tropical cyclone, a large fraction of the energy is partitioned to gravity-inertia wave motion.[1] This leads us to the view that under certain circumstances tropical cyclones may be highly radiating systems. Consequently, if the process of geostrophic or gradient adjustment is to be properly represented, it is essential that the lateral boundary condition be able to transmit the gravity-inertia wave energy generated by the release of latent heat in the interior of the model.

There are two broad classes of tropical cyclone models: balanced models and primitive equation models. In a balanced model (e.g., Ogura, 1964; Kuo, 1965; Ooyama, 1969a,b; Sundqvist, 1970a,b) the flow is assumed to be axisymmetric and in gradient wind balance. Since gravity-inertia waves are then filtered, the transient aspects of the geostrophic adjustment[2] process are not simulated. Primitive equation models, however, may be axisymmetric (e.g. Yamasaki, 1968a,b; Rosenthal, 1970, 1971, 1978; Kurihara, 1975) or asymmetric (e.g. Anthes *et al.*, 1971a,b; Anthes, 1972; Harrison, 1973; Kurihara and Tuleya, 1974; Mathur, 1974; Madala and Piacsek, 1975; Jones, 1977; Kurihara *et al.*, 1979) and in either case the geostrophic adjustment process becomes one of the important physical processes which must be accurately simulated. Because of their filtered nature, the formulation of lateral boundary conditions in balanced models is not so difficult. Discussions of this problem can be found in Ooyama (1969a) and Sundqvist (1970a). In this paper, we will concentrate on lateral boundary conditions for axisymmetric primitive equation models, noting that the generalization of our results to the asymmetric case is not difficult.

[1]Examples of this energy partition for axisymmetric flow on an f plane can be found in Section 4 of this paper and in Schubert *et al.* (1980). Examples on the equatorial β plane can be found in Silva Dias, P. L., and W. H. Schubert, 1979: The dynamics of equatorial mass-flow adjustment. Atmos. Sci. Pap. No. 312, Colorado State University.

[2]We shall henceforth use the term geostrophic adjustment in the broad sense of adjustment to either geostrophic or gradient balance.

0027-0644/81/071404-17$08.25

A survey of the literature on primitive equation tropical cyclone models indicates that the lateral boundary conditions on the normal wind component which have been used involve either the condition of zero divergence (Rosenthal, 1970; Anthes, 1971, 1977; Anthes *et al.*, 1971a,b; Jones, 1977) or the condition of zero radial wind (Yamasaki, 1968a,b; Kurihara and Tuleya, 1974; Kurihara, 1975; Rosenthal, 1978). Rosenthal (1971) has examined the sensitivity of an axisymmetric primitive equation tropical cyclone model to these two boundary conditions as functions of the computational domain size. Results of the numerical integrations indicated that the maximum surface winds attained in those experiments incorporating the condition of zero divergence were relatively insensitive to the size of the domain. In contrast, when using the condition of zero radial wind, the model produced weaker surface winds which were highly sensitive to the size of the computational domain such that there was a linear increase of the maximum surface wind with domain size. Rosenthal's conclusion is that by enlarging the computational domain to somewhere between 2000 and 3000 km, differences in the numerical result attributable to differences in boundary conditions can be minimized.

In this paper we shall approach the problem of lateral boundary conditions from a different, essentially linear, point of view, with the goal of minimizing the reflection of gravity-inertia waves, and consequently the distortion of the geostrophic adjustment process. We shall show that such false reflections can be controlled by the use of a gravity wave radiation condition, if the condition is applied separately to each vertical mode. The application of an interface boundary condition to selected vertical modes has been discussed for limited area nested forecast models by Elvius (1977).

Since many primitive equation tropical cyclone models are based on the sigma coordinate, we derive in Section 2 a linearized system of equations formulated in this coordinate. The linearized system can be transformed in the vertical which essentially splits the problem into two parts: a vertical structure problem and a horizontal structure problem. In Section 3 we solve the vertical structure problem, obtaining the eigenvalues and associated vertical structure functions for both an atmosphere characterized by a constant static stability and a mean tropical static stability. Using these results, we explore in Section 4 the energy partition between geostrophic flow and gravity-inertia waves for a given forcing in the mass field. The conclusion is that for certain combinations of the space and time scales of the forcing the majority of the generated energy is partitioned to outward propagating gravity-inertia waves. This motivates a search for a radiation condition which has low reflectivity (Section 5). Since the boundary condition found in Section 5 is only an approximate condition, its usefulness is explored numerically (Section 6) by comparing it with several other conditions, including those recently proposed for use in convection models by Orlanski (1976) and Klemp and Wilhelmson (1978).

2. Governing equations

We begin by considering the equations which govern axisymmetric flow, using cylindrical coordinates in the horizontal and the σ-coordinate in the vertical. Following Arakawa and Lamb (1977) we define σ as

$$\sigma \equiv \frac{p - p_T}{p_S - p_T} \equiv \frac{p - p_T}{\pi}, \tag{2.1}$$

where the top boundary pressure p_T is a specified constant, and the surface pressure p_S (or equivalently π) is a function of the horizontal coordinate and time. The upper and lower boundaries are given by $\sigma = 0$ and $\sigma = 1$, respectively. In the special case where $p_T = 0$, (2.1) reduces to the definition originally proposed by Phillips (1957).

The governing equations, which consist of the horizontal momentum equations, the hydrostatic equation, the mass continuity equation, the thermodynamic equation and the ideal gas law can be written

$$\frac{du}{dt} - \left(f + \frac{v}{r}\right)v + \frac{\partial \phi}{\partial r} + \sigma\alpha\frac{\partial \pi}{\partial r} = F, \tag{2.2}$$

$$\frac{dv}{dt} + \left(f + \frac{v}{r}\right)u = G, \tag{2.3}$$

$$\frac{\partial \phi}{\partial \sigma} = -\pi\alpha, \tag{2.4}$$

$$\frac{d\pi}{dt} + \pi\left(\frac{\partial ru}{r\partial r} + \frac{\partial \dot{\sigma}}{\partial \sigma}\right) = 0, \tag{2.5}$$

$$\frac{dT}{dt} - \frac{\kappa T}{p}\frac{dp}{dt} = \frac{Q}{c_p}, \tag{2.6}$$

$$p\alpha = RT, \tag{2.7}$$

where F and G are apparent momentum source/sink terms (including cumulus effects), Q is the apparent heat source, $d/dt = \partial/\partial t + u(\partial/\partial r) + \dot{\sigma}(\partial/\partial\sigma)$ is the time derivative following the transverse motion, and where the vertical σ velocity is defined by $\dot{\sigma} = d\sigma/dt$. As upper and lower boundary conditions we require that fluid particles do not cross the $\sigma = 0$ and $\sigma = 1$ surfaces, i.e.,

$$\dot{\sigma} = 0 \quad \text{at} \quad \sigma = 0, 1. \tag{2.8}$$

For the purpose of our analysis it is more con-

venient to consider the linear version of (2.2)–(2.7). Linearizing this system about a basic state (denoted by overbars) which is at rest, we obtain

$$\frac{\partial u}{\partial t} - fv + \frac{\partial}{\partial r}(\phi + \sigma\bar{\alpha}\pi) = F, \tag{2.9}$$

$$\frac{\partial v}{\partial t} + fu = G, \tag{2.10}$$

$$\frac{\partial \pi}{\partial t} + \bar{\pi}\left(\frac{\partial ru}{r\partial r} + \frac{\partial \dot{\sigma}}{\partial \sigma}\right) = 0, \tag{2.11}$$

$$\frac{\partial}{\partial t}\left[\frac{\partial \phi}{\partial \sigma} + \left(1 - \frac{\sigma\bar{\pi}}{\gamma\bar{p}}\right)\bar{\alpha}\,\pi\right] + S\dot{\sigma} = -\frac{R\bar{\pi}}{\bar{p}}\frac{Q}{c_p}, \tag{2.12}$$

where $\gamma = c_p/c_v$ and the basic-state static stability has been defined as

$$S \equiv \frac{R\bar{\pi}}{\bar{p}}\left(\frac{\bar{\pi}\,\bar{\alpha}}{c_p} - \frac{d\bar{T}}{d\sigma}\right).$$

Following the approach of Robert *et al.* (1972), Daley (1979), Temperton and Williamson (1979)[3] and Kasahara and Puri (1981), we define two new dependent variables Φ and ω by

$$\Phi = \phi + \sigma\,\bar{\alpha}\,\pi, \tag{2.13a}$$

$$\omega = \bar{\pi}\,\dot{\sigma} + \sigma\frac{\partial \pi}{\partial t}. \tag{2.13b}$$

The use of (2.13) in (2.9)–(2.12), followed by the elimination of ω, leads to

$$\frac{\partial u}{\partial t} - fv + \frac{\partial \Phi}{\partial r} = \frac{\partial \tilde{u}}{\partial t}, \tag{2.14}$$

$$\frac{\partial v}{\partial t} + fu = \frac{\partial \tilde{v}}{\partial t}, \tag{2.15}$$

$$\frac{\partial}{\partial t}\left[\frac{\partial}{\partial \sigma}\left(\frac{1}{S}\frac{\partial \Phi}{\partial \sigma}\right)\right] - \frac{\partial ru}{r\partial r} = \frac{\partial}{\partial t}\left[\frac{\partial}{\partial \sigma}\left(\frac{1}{S}\frac{\partial \tilde{\Phi}}{\partial \sigma}\right)\right], \tag{2.16}$$

where we have defined

$$\frac{\partial \tilde{u}}{\partial t} \equiv F, \quad \frac{\partial \tilde{v}}{\partial t} \equiv G \quad \text{and} \quad \frac{\partial}{\partial t}\left(\frac{\partial \tilde{\Phi}}{\partial \sigma}\right) \equiv -\frac{R\bar{\pi}}{\bar{p}}\frac{Q}{c_p}.$$

The variable $\tilde{\Phi}$, for example, can be interpreted as the "geopotential" which would result if the atmosphere were not allowed to adjust to the forcing (i.e., if the vertical motion field were constrained to be zero). The boundary conditions (2.8), when expressed in terms of Φ and $\tilde{\Phi}$ become[4]

$$\frac{\partial}{\partial t}\left[\frac{\partial}{\partial \sigma}(\Phi - \tilde{\Phi})\right] = 0 \quad \text{at} \quad \sigma = 0, \tag{2.17a}$$

$$\frac{\partial}{\partial t}\left[\frac{\partial}{\partial \sigma}(\Phi - \tilde{\Phi}) + \frac{S}{\bar{\pi}\,\bar{\alpha}}(\Phi - \tilde{\Phi})\right] = 0 \quad \text{at} \quad \sigma = 1. \tag{2.17b}$$

Thus, the governing system of linear equations consists of (2.14)–(2.16) in the unknowns u, v and Φ subject to the boundary conditions (2.17).

For any function $\chi(r,\sigma,t)$, we introduce the vertical transform pair

$$\chi_n(r,t) = \int_0^1 \chi(r,\sigma,t)\,\Psi_n(\sigma)\,d\sigma, \tag{2.18}$$

$$\chi(r,\sigma,t) = \sum_n \chi_n(r,t)\,\Psi_n(\sigma), \tag{2.19}$$

where the kernel $\Psi_n(\sigma)$ satisfies a yet to be determined Sturm-Liouville problem. The vertical transform of (2.14) and (2.15) is easily accomplished while (2.16) requires integration by parts, use of boundary conditions (2.17), and the determination of the differential equation and boundary conditions for $\Psi_n(\sigma)$. The transformed equations are given by

$$\frac{\partial u_n}{\partial t} - fv_n + \frac{\partial \Phi_n}{\partial r} = \frac{\partial \tilde{u}_n}{\partial t}, \tag{2.20}$$

$$\frac{\partial v_n}{\partial t} + fu_n = \frac{\partial \tilde{v}_n}{\partial t}, \tag{2.21}$$

$$\frac{\partial \Phi_n}{\partial t} + gh_n\frac{\partial ru_n}{r\partial r} = \frac{\partial \tilde{\Phi}_n}{\partial t}, \tag{2.22}$$

where the kernel $\Psi_n(\sigma)$ satisfies

$$\frac{d}{d\sigma}\left(\frac{1}{S}\frac{d\Psi_n}{d\sigma}\right) + \frac{1}{gh_n}\Psi_n = 0, \tag{2.23}$$

subject to

$$\frac{d\Psi_n}{d\sigma} = 0 \quad \text{at} \quad \sigma = 0, \tag{2.24a}$$

$$\frac{d\Psi_n}{d\sigma} + \frac{S}{\bar{\pi}\,\bar{\alpha}}\Psi_n = 0 \quad \text{at} \quad \sigma = 1. \tag{2.24b}$$

Eq. (2.23) can be considered the vertical structure equation for our problem and, along with boundary conditions (2.24), gives rise to a countably infinite set of eigenvalues gh_n, and a corresponding set of eigenfunctions (vertical structure or basis functions) $\Psi_n(\sigma)$. Since (2.23) and (2.24) constitute a Sturm-Liouville problem, the vertical

[3]Temperton, C., and D. L. Williamson, 1979: Normal mode initialization for a multi-level gridpoint model. Tech. Rep. No. 11, European Centre for Medium Range Weather Forecasts, Shinfield Park, Reading, England.

[4]We also assume $\tilde{\Phi} = 0$ at $\sigma = 1$.

structure functions $\Psi_n(\sigma)$ form a complete and orthogonal set on the interval [0,1]. They also may be normalized so that

$$\int_0^1 \Psi_m(\sigma)\,\Psi_n(\sigma)\,d\sigma = \begin{cases} 1, & m = n \\ 0, & m \neq n. \end{cases} \quad (2.25)$$

We shall present some solutions of (2.23) and (2.24) in Section 3.

The linear system (2.20)–(2.22) constitutes the horizontal structure problem and is more commonly referred to as the divergent barotropic system of equations, or the shallow-water equations. In their simplest context (2.20)–(2.22) govern small-amplitude perturbations in a rotating, homogeneous, incompressible and hydrostatic fluid with a mean free surface height h_n. We note that the phase speed of a pure gravity wave in such a fluid is given by $(gh_n)^{1/2}$. For the more general stratified problem (2.20)–(2.22) govern the behavior of each of the vertical structure functions arising from the solution of (2.23) and (2.24). Consequently, the eigenvalue $(gh_n)^{1/2} \equiv c_n$, where h_n is known as the equivalent depth, is interpreted as the pure gravity wave phase velocity of the associated vertical mode $\Psi_n(\sigma)$. In Section 5 we shall use (2.20)–(2.22) to determine an approximate boundary condition and to examine the reflectivity of boundary conditions in general.

3. Analysis of the vertical structure problem

The solution of (2.23) and (2.24) requires the specification of the basic state static stability. The simplest case that can be considered is one in which the static stability is a constant. For such a situation the normalized basis functions Ψ_n are given by

$$\Psi_n(\sigma) = \left(\frac{2}{1 + (2\lambda_n)^{-1}\sin 2\lambda_n}\right)^{1/2} \cos\lambda_n\sigma, \quad (3.1)$$

where $\lambda_n \equiv (S/gh_n)^{1/2}$ is determined from the eigenvalue relation

$$\lambda_n \tan\lambda_n = \frac{S}{\bar{\pi}\,\bar{\alpha}(1)}, \quad n = 0, 1, 2, \ldots. \quad (3.2)$$

A good approximation to (3.2) is

$$\left.\begin{aligned} c_0 &= (gh_0)^{1/2} \approx [\bar{\pi}\,\bar{\alpha}(1)]^{1/2} \\ c_n &= (gh_n)^{1/2} \approx \frac{S^{1/2}}{n\pi} \quad \text{for} \quad n = 1, 2, 3, \ldots \end{aligned}\right\}. \quad (3.3)$$

We see from this approximation that except for the external mode ($n = 0$), the eigenvalues c_n are proportional to $1/n$. The first 18 exact and approximate eigenvalues, determined from (3.2) and (3.3), respectively, are listed in Table 1. These results are based on $\bar{\pi} = 90$ kPa, $\bar{\alpha}(1) = 0.861$ m^3 kg^{-1}, and $S^{1/2} = 162.77$ m s^{-1}. The first five basis functions determined from (3.1) and (3.2) are shown in Fig. 1a. These basis functions give the vertical structure of the dependent variables u, v and Φ. The variable ω has a vertical structure proportional to $-\lambda_n^{-1}(d\Psi_n/d\sigma)$, which is plotted for the first five modes in Fig. 2a.

TABLE 1. The first 18 exact and approximate eigenvalues c_n, determined from Eqs. (3.2) and (3.3) for the constant static stability case, and numerically for the static stability profile of Fig. 3. Units are m s^{-1}.

Vertical mode n	Constant static stability: Eq. (3.2) (exact)	Constant static stability: Eq. (3.3) (approximate)	Static stability of Fig. 3
0	294.15	278.39	287.55
1	50.14	51.81	51.61
2	25.69	25.91	26.81
3	17.21	17.27	19.40
4	12.93	12.95	14.81
5	10.35	10.36	11.80
6	8.63	8.64	9.77
7	7.40	7.40	8.39
8	6.47	6.48	7.42
9	5.75	5.76	6.64
10	5.18	5.18	6.02
11	4.71	4.71	5.49
12	4.32	4.32	5.04
13	3.99	3.99	4.65
14	3.70	3.70	4.31
15	3.45	3.45	4.02
16	3.24	3.24	3.76
17	3.05	3.05	3.53

In the tropical atmosphere the basic state static stability varies considerably. This is illustrated in Fig. 3 where the vertical profile of $S^{1/2}$ was calculated from the mean tropical clear area temperature profile of Gray *et al.* (1975). The constant value of $S^{1/2}$ used in the earlier calculations is indicated by the vertical dashed line. The vertical structure problem (2.24) and (2.25) can be solved numerically for this more realistic $S^{1/2}$ profile. The eigenvalues which are obtained are shown in the last column of Table 1, and the basis functions Ψ_n and $-\lambda_n^{-1}(d\Psi_n/d\sigma)$ are shown in Figs. 1b and 2b, respectively. We see that the effect of the variable static stability is primarily to increase the propagation speeds of the higher order vertical modes. This is probably a consequence of the large values of $S^{1/2}$ in the upper troposphere. We also note that the vertical structure functions are modified in this region of high static stability, such that the vertical wavelengths are shortened and the amplitudes are increased.

4. Importance of the lateral boundary condition

Before considering several lateral boundary conditions in the next section, we attempt to establish the importance of carefully formulated lateral boundary conditions in tropical cyclone models. The argument presented in this section is that when latent heat is released on horizontal scales typical

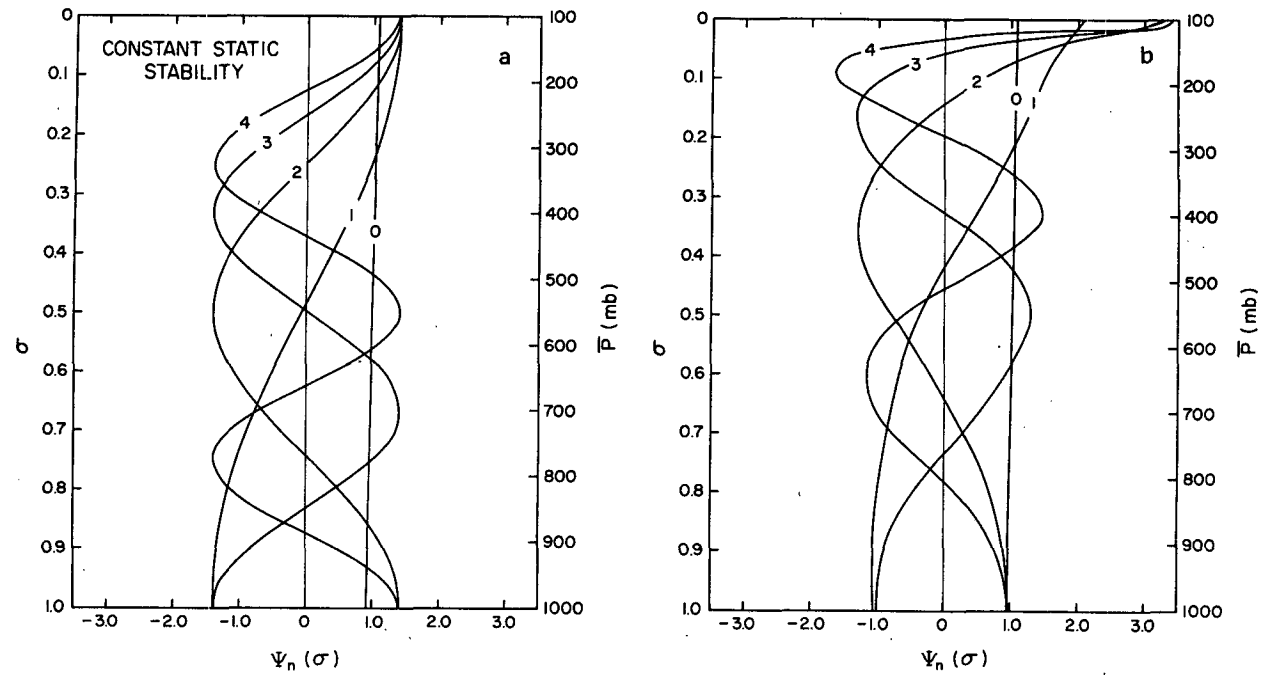

FIG. 1. Eigenfunctions $\psi_n(\sigma)$ for (a) constant static stability and (b) the static stability profile of Fig. 3.

of a tropical cyclone and on time scales shorter than the local adjustment time scale only a small fraction of the released latent energy ends up in balanced flow. The major portion of this energy is partitioned to outward propagating gravity-inertia waves. This lopsided energy partition can be illustrated with a simple example.

From (2.21) and (2.22) we can derive the potential vorticity equation

$$\frac{\partial}{\partial t}\left(\frac{\partial r v_n}{r\partial r} - \frac{f}{c_n^2}\Phi_n\right) = \frac{\partial}{\partial t}\left(\frac{\partial r \tilde{v}_n}{r\partial r} - \frac{f}{c_n^2}\Phi_n\right). \quad (4.1)$$

Integrating (4.1), assuming that $v_n(r,0) = \tilde{v}_n(r,t) =$

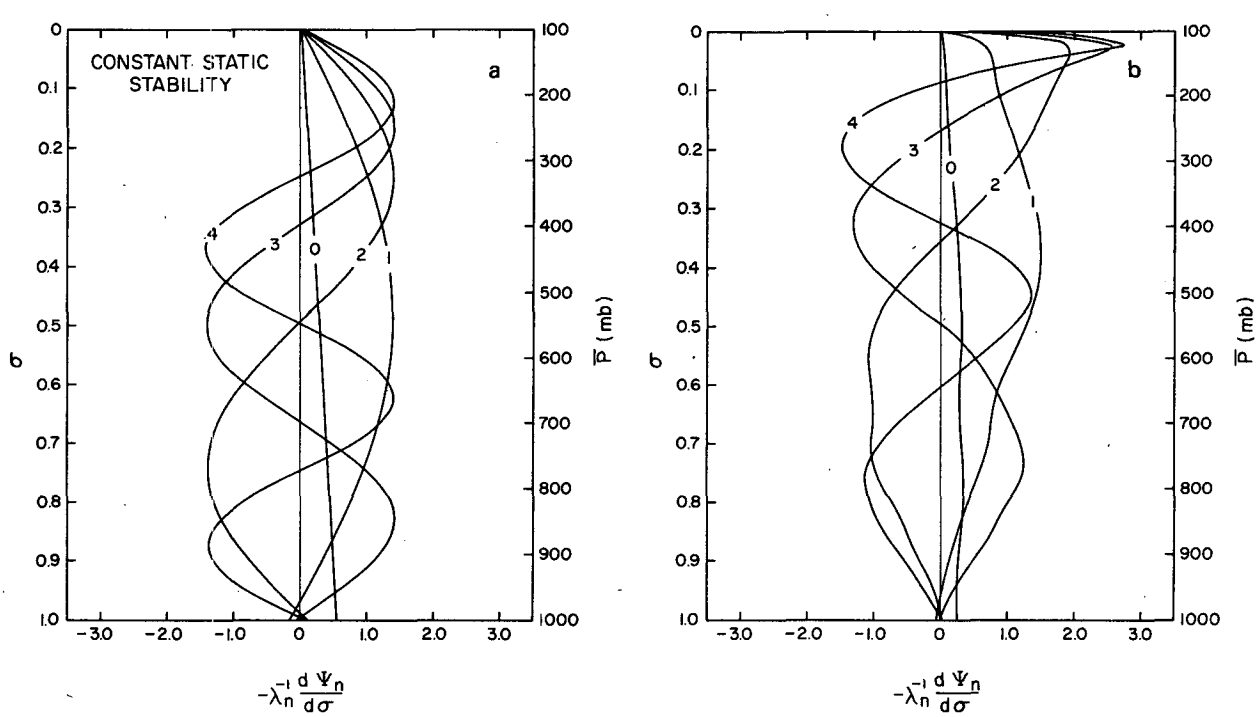

FIG. 2. Vertical profiles of $-\lambda_n^{-1}d\Psi_n/d\sigma$ for (a) constant static stability and (b) the static stability profile of Fig. 3.

$\Phi_n(r,0) = \tilde{\Phi}_n(r,0) = 0$, that the time integrated heating results in

$$\tilde{\Phi}(r,\infty) = \begin{cases} c_n^2, & r < a \\ 0, & r > a, \end{cases} \tag{4.2}$$

and that the final flow is geostrophic, we obtain

$$\frac{d^2\Phi_n(r,\infty)}{dr^2} + \frac{d\Phi_n(r,\infty)}{rdr} - \frac{f^2}{c_n^2}\Phi_n(r,\infty) = \begin{cases} f^2, & r < a \\ 0, & r > a. \end{cases} \tag{4.3}$$

The solution of (4.3) which remains bounded at the origin and at infinity and which possesses continuous $\Phi_n(r,\infty)$ and $v_n(r,\infty)$ at $r = a$ is

$$\frac{\Phi_n(r,\infty)}{c_n^2} = \begin{cases} \dfrac{fa}{c_n} K_1\left(\dfrac{fa}{c_n}\right) I_0\left(\dfrac{fr}{c_n}\right) - 1, & r < a \\ -\dfrac{fa}{c_n} I_1\left(\dfrac{fa}{c_n}\right) K_0\left(\dfrac{fr}{c_n}\right), & r \geq a, \end{cases} \tag{4.4}$$

where I_m and K_m are the order m modified Bessel functions.

The sum of the kinetic and the available potential energy associated with the final geostrophic flow, $K_\infty + P_\infty$, can be obtained by multiplying (4.3) by $\Phi_n(r,\infty)$ and integrating over area. The result is

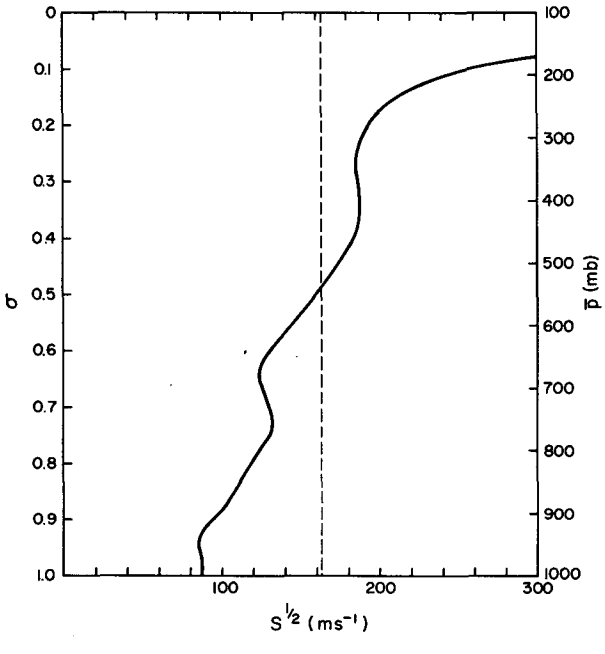

FIG. 3. Square root of the basic state static stability computed from the mean tropical clear area temperature profile of Gray *et al.* (1975).

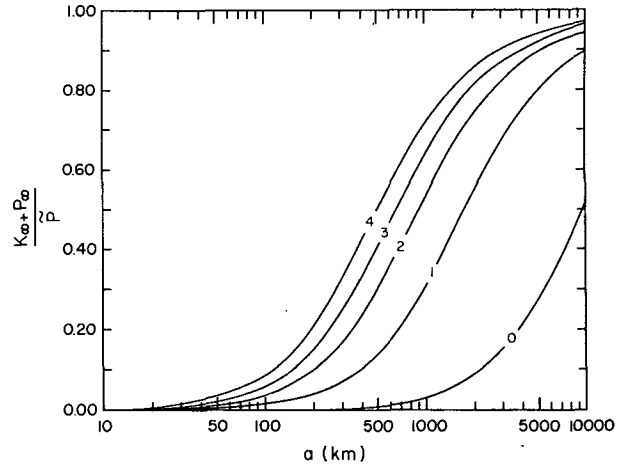

FIG. 4. The fraction of the available potential energy associated with $\tilde{\Phi}(r,\infty)$ which is partitioned to geostrophic flow as a function of the horizontal scale of the geopotential forcing. The curves have been computed using (4.6) for the first five values of c_n given in the last column of Table 1 and for an f corresponding to a latitude of 20°N.

$$K_\infty + P_\infty = \int_0^\infty \tfrac{1}{2}[v_n^2(r,\infty) + c_n^{-2}\Phi_n^2(r,\infty)]\, rdr$$

$$= \tfrac{1}{2}c_n^{-2}\int_0^\infty \Phi_n(r,\infty)\,\tilde{\Phi}_n(r,\infty)\, rdr. \tag{4.5}$$

Substituting (4.2) and (4.4) into (4.5) and normalizing by the available potential energy associated with $\tilde{\Phi}_n(r,\infty)$ we obtain

$$\frac{K_\infty + P_\infty}{\tilde{P}} = 1 - 2K_1\left(\frac{fa}{c_n}\right) I_1\left(\frac{fa}{c_n}\right). \tag{4.6}$$

The energy ratio $(K_\infty + P_\infty)/\tilde{P}$ yields a single curve if we plot it as a function of the dimensionless horizontal scale fa/c_n. However for convenient physical interpretation, we have plotted in Fig. 4 the energy ratio as a function of the dimensional horizontal scale a, at 20°N, for the first five values of c_n given in the last column of Table 1. Fig. 4 needs to be interpreted with some caution since the normalization factor $\tilde{P}$ should not be regarded as the available potential energy which has been generated by latent heat release. Rather it is the available potential energy which would have been generated if all the heating had gone into local thickness change. In order to determine the available potential energy actually generated by the heating, it would be necessary to compute the time integral of the product of the geopotential and the heating, which is beyond the scope of the simple potential vorticity argument presented in this section. However, if the atmosphere were to be heated on a time scale shorter than the local adjustment time scale (on the order of $[(f + \bar{\zeta})(f + 2\bar{v}/r)]^{-1/2}$ for the more general case in which a non-resting vertically independent basic

state flow is included) a large fraction of the heating would go into local thickness change and a large generation of available potential energy would occur. In the limiting case of impulsive heating $\bar{P}$ can be considered the amount of available potential energy generated by the heating and for such a situation the difference between $(K_\infty + P_\infty)/\bar{P}$ and unity (Fig. 4) represents the fraction of the generated energy partitioned to outward propagating gravity-inertia waves. We see that for horizontal scales ≤ 300 km, the majority of the impulsively generated energy is partitioned to gravity-inertia wave motion. Although this argument is strictly valid only for impulsive heating, it is approximately true for heating with time scales shorter than the local adjustment time scale. In light of the large amounts of latent heat released in tropical storms it would be reasonable to conclude that gravity-inertia wave energy leaving the vicinity of a tropical cyclone could be substantial, especially for the low-order vertical modes. Although the energy ratio curves shown in Fig. 4 depend on the horizontal structure of the chosen forcing, these curves are typical of other examples we have investigated (Schubert *et al.*, 1980). They show the very low efficiency of geostrophic energy generation by tropical cyclone scale heating in low latitudes and lead naturally to the view that, in terms of gravity-inertia wave energy, tropical cyclones may, at times, be highly radiating systems.

There are, of course, real physical situations in which gravity-inertia waves might be reflected back toward their source. However, the imposition of a lateral boundary to the computational domain of a numerical model should not result in the reflection of incident waves. Improper reflection of gravity-inertia waves in a model which carries water vapor as a dependent variable can become intolerable since the vertical motion field associated with these reflected waves (see Fig. 2b) can interact nonlinearly with the moisture field to produce an erroneous pattern of latent heat release. Consequently, a poorly formulated lateral boundary condition can indirectly contribute to significant alterations of the numerical solution, especially with regard to the transient behavior of the simulated disturbance.

5. Analysis of the horizontal structure problem

a. An exact boundary condition

A fairly thorough study of open-boundary conditions for dispersive waves has been conducted by Bennett (1976). We apply his approach to our problem by considering the horizontal structure equations (2.20)–(2.22) for the vertical mode n. Defining $\hat{\chi}_n(r,s)$ as the Laplace transform of $\chi_n(r,t)$ and assuming no initial disturbance and no source/sink terms for $r \geq a$, we transform (2.20)–(2.22) and eliminate $\hat{\Phi}_n(r,s)$ and $\hat{v}_n(r,s)$ to obtain

$$r^2 \frac{d^2\hat{u}_n}{dr^2} + r\frac{d\hat{u}_n}{dr} - \left[\left(\frac{s^2+f^2}{c_n^2}\right) r^2 + 1\right]\hat{u}_n = 0 \quad \text{for} \quad r \geq a. \tag{5.1}$$

The solution of (5.1) which remains bounded as $r \to \infty$ is given by

$$\hat{u}_n(r,s) = A(s)\, K_1\left[\left(\frac{s^2+f^2}{c_n^2}\right)^{1/2} r\right] \quad \text{for} \quad r \geq a. \tag{5.2}$$

It can be shown that the transformed radial wind component $\hat{u}_n(r,s)$ also satisfies

$$\frac{dr\hat{u}_n}{dr} = \frac{\dfrac{d}{dr}\left\{rK_1\left[\left(\dfrac{s^2+f^2}{c_n^2}\right)^{1/2} r\right]\right\}}{K_1\left[\left(\dfrac{s^2+f^2}{c_n^2}\right)^{1/2} r\right]}\hat{u}_n \quad \text{at} \quad r = a. \tag{5.3}$$

In a balanced tropical cyclone model the first term in (2.14) is neglected. For such a model (5.3) remains unchanged except for the omission of s^2. In this special case (5.3) can be inverted to give

$$\frac{\partial r u_n}{\partial r} = -\frac{fa}{c_n}\left[\frac{K_0(fa/c_n)}{K_1(fa/c_n)}\right] u_n \quad \text{at} \quad r = a. \tag{5.4}$$

This is the proper boundary condition for forced rotational modes, which are the only modes appearing in a balanced model. Boundary condition (5.4) has been used by Ooyama (1969a) for the upper level radial flow in his three-layer model. It has also been used by Sundqvist (1970a) at each level of his ten-level model with a value of c_n corresponding to the first internal mode.

An exact boundary condition for both rotational and gravitational modes can be obtained by inverting (5.3). Unfortunately, this procedure yields an expression which is quite complicated and of questionable practical value. This is more readily illustrated if we utilize the large argument asymptotic form of the modified Bessel function K_1 to simplify (5.3) to

$$(s^2+f^2)^{1/2}\hat{u}_n + c_n \frac{\partial r^{1/2}\hat{u}_n}{r^{1/2}\partial r} = 0 \quad \text{at} \quad r = a, \tag{5.5}$$

which, when multiplied by $s(s^2+f^2)^{-1/2}$, can be inverted to give

$$\frac{\partial u_n(r,t)}{\partial t} + c_n \frac{\partial r^{1/2}u_n(r,t)}{r^{1/2}\partial r} = f c_n \int_0^t J_1[f(t-t')] \times \frac{\partial r^{1/2}u_n(r,t')}{r^{1/2}\partial r}\, dt' \quad \text{at} \quad r = a. \tag{5.6}$$

Relationships of this kind require that we store and

repeatedly sum (with different weights) boundary values of u_n and its horizontal derivative. The storage requirements alone are effectively equivalent to allowing the computational domain to expand in time. Since this is what we are attempting to avoid, the idea of using an exact boundary condition must be abandoned for practical reasons.

Because of the difficulties involved in applying (5.6) we consider the two limiting cases of (5.5), $s \gg f$, which when inverted can be written

$$\frac{\partial u_n}{\partial t} + c_n \frac{\partial r^{1/2} u_n}{r^{1/2} \partial r} = 0 \quad \text{at} \quad r = a, \tag{5.7}$$

and $f \gg s$, which can be inverted to give

$$f u_n + c_n \frac{\partial r^{1/2} u_n}{r^{1/2} \partial r} = 0 \quad \text{at} \quad r = a. \tag{5.8}$$

Eq. (5.7) can be regarded as an asymptotically valid radiation condition for pure gravity waves and will be discussed further in Section 5b. Eq. (5.8) represents an asymptotically valid boundary condition for balanced flow (i.e., for forced rotational modes) and is simply an approximate version of (5.4). The use of (5.8) instead of (5.4) can be justified if the boundary radius is larger than the Rossby radius c_n/f. Although this is usually true for the internal modes, it is practically never the case for the external mode. It might be argued that during model integration one should choose between (5.7) and (5.8) [or more precisely (5.4)] based on the relative magnitudes of $\partial u_n/\partial t$ and $f u_n$. We shall not explore this possibility but rather concentrate on the usefulness of (5.7) alone.

b. *Reflectivity analysis*

A more conventional method of studying boundary conditions is through a reflectivity analysis. We begin such an analysis by noting that the system (2.20)–(2.22) has solutions of the form

$$\begin{bmatrix} u_n(r,t) \\ v_n(r,t) \\ \Phi_n(r,t) \end{bmatrix} \propto \begin{bmatrix} 1 \\ -\dfrac{if}{\nu_n} \\ -\dfrac{ic_n{}^2 k}{\nu_n} \end{bmatrix} \times \left\{ \begin{bmatrix} H_1^{(1)}(kr) \\ H_1^{(1)}(kr) \\ H_0^{(1)}(kr) \end{bmatrix} + R \begin{bmatrix} H_1^{(2)}(kr) \\ H_1^{(2)}(kr) \\ H_0^{(2)}(kr) \end{bmatrix} \right\} e^{-i\nu_n t}, \tag{5.9}$$

where the frequency ν_n is given by $\nu_n = (f^2 + c_n{}^2 k^2)^{1/2}$, k is the horizontal wavenumber, R is a complex constant, and $H_m^{(1)}(kr)$ and $H_m^{(2)}(kr)$ are the order m Hankel functions of the first and second kind. The use of asymptotic expansions valid for large kr allows (5.9) to be written

$$\begin{bmatrix} u_n(r,t) \\ v_n(r,t) \\ \Phi_n(r,t) \end{bmatrix} \sim \left(\frac{2}{\pi k r}\right)^{1/2} e^{-3\pi i/4} \times \begin{bmatrix} 1 \\ -\dfrac{if}{\nu_n} \\ \dfrac{c_n{}^2 k}{\nu_n} \end{bmatrix} \left\{ e^{i(kr - \nu_n t)} - iRe^{-i(kr + \nu_n t)} \right\}. \tag{5.10}$$

The first term in both (5.9) and (5.10) corresponds to an outward propagating wave while the second term corresponds to an inward propagating wave. Thus, at large radius a (the radius of the model boundary), the asymptotic form of the outward propagating wave satisfies the radiation condition[5]

$$\frac{\partial u_n}{\partial t} + \frac{\nu_n}{k} \frac{\partial r^{1/2} u_n}{r^{1/2} \partial r} = 0 \quad \text{at} \quad r = a. \tag{I}$$

If a disturbance in the form of a wave packet centered on wavenumber k approaches the boundary, the use of boundary condition I should result in low reflectivity as long as $ka \gg 1$. The primary disadvantage of I is that it is difficult to apply in physical space because knowledge of ν_n/k is required. However, since $\nu_n/k \to c_n$ as $k \to \infty$, we might approximate I by

$$\frac{\partial u_n}{\partial t} + c_n \frac{\partial r^{1/2} u_n}{r^{1/2} \partial r} = 0 \quad \text{at} \quad r = a, \tag{II}$$

which is identical to (5.7) and which is much easier to apply in physical space because c_n is known from the solution of the vertical structure problem. This approximation is equivalent to neglecting the Coriolis parameter and confining our study to nondispersive or pure gravity wave motion. One additional approximation can be made to II, and that is to neglect the effects of cylindrical geometry, which gives

$$\frac{\partial u_n}{\partial t} + c_n \frac{\partial u_n}{\partial r} = 0 \quad \text{at} \quad r = a. \tag{III}$$

Let us also consider the two most widely used boundary conditions in tropical cyclone models which are the condition of zero divergence,

[5]Boundary condition (I) bears a certain equivalence to (5.6) since both involve asymptotic approximations to Bessel functions.

TABLE 2. Reflectivities for boundary conditions I–V.

Boundary condition	Reflectivity
(I) $\frac{\partial u_n}{\partial t} + \frac{\nu_n}{k}\frac{\partial r^{1/2}u_n}{r^{1/2}\partial r} = 0$	$\lvert R\rvert = \dfrac{\left\lvert H_0^{(1)}(ka) - \left(\frac{1}{2ka} + i\right)H_1^{(1)}(ka)\right\rvert}{\left\lvert H_0^{(2)}(ka) - \left(\frac{1}{2ka} + i\right)H_1^{(2)}(ka)\right\rvert}$
(II) $\frac{\partial u_n}{\partial t} + c_n\frac{\partial r^{1/2}u_n}{r^{1/2}\partial r} = 0$	$\lvert R\rvert = \dfrac{\left\lvert H_0^{(1)}(ka) - \left(\frac{1}{2ka} + \frac{i\nu_n}{c_nk}\right)H_1^{(1)}(ka)\right\rvert}{\left\lvert H_0^{(2)}(ka) - \left(\frac{1}{2ka} + \frac{i\nu_n}{c_nk}\right)H_1^{(2)}(ka)\right\rvert}$
(III) $\frac{\partial u_n}{\partial t} + c_n\frac{\partial u_n}{\partial r} = 0$	$\lvert R\rvert = \dfrac{\left\lvert H_0^{(1)}(ka) - \left(\frac{1}{ka} + \frac{i\nu_n}{c_nk}\right)H_1^{(1)}(ka)\right\rvert}{\left\lvert H_0^{(2)}(ka) - \left(\frac{1}{ka} + \frac{i\nu_n}{c_nk}\right)H_1^{(2)}(ka)\right\rvert}$
(IV) $\frac{\partial ru_n}{r\partial r} = 0$	$\lvert R\rvert = 1$
(V) $u_n = 0$	$\lvert R\rvert = 1$

$$\frac{\partial ru_n}{r\partial r} = 0 \quad \text{at} \quad r = a, \tag{IV}$$

and the condition of zero radial wind,

$$u_n = 0 \quad \text{at} \quad r = a. \tag{V}$$

The reflectivity of each of the conditions I–V can be found by substituting (5.9) and solving for $|R|$.[6] The mathematical expressions are given in Table 2. Since conditions IV and V have unit reflectivity and the reflectivity of III is larger than II (Schubert *et al.*, 1980), we confine the remainder of this discussion to a comparison of I and II. As can be seen from Table 2 the reflectivity of boundary condition II is a function of both ka and ν_n/c_nk. In Fig. 5 we have drawn isopleths of $|R|$ in the $[ka, \nu_n/c_nk]$ plane for boundary condition II. From Fig. 5 one also can obtain the reflectivity of I since it is identical to the reflectivity of II along the line $\nu_n/c_nk = 1$. As long as c_n is within about 10% of ν_n/k and $ka \gtrsim 1.5$, the reflectivity can be held under 5%.

In order to understand the implications of the reflectivity relations for a particular model situation, it is more convenient to display the results in dimensional form. The reflectivities of the 18 vertical modes which have the eigenvalues listed in the last column of Table 1 are illustrated in Fig. 6 for boundary condition II. These reflectivities are calculated for a domain size of 960 km, and for an f corresponding to a latitude of 20°N. We see that, for a given wavenumber k, a larger fraction of the incident wave is reflected as the vertical mode is increased. This result is due to the fact that the higher order modes propagate at a slower rate and hence have longer periods. Thus, the Coriolis force plays a larger role in the dynamics of these waves, but is neglected in the boundary condition since ν_n/k has been approximated by its pure gravity wave value c_n. Accordingly, boundary condition II is mode dependent, while boundary condition I is mode independent, its reflection curve being indistinguishable

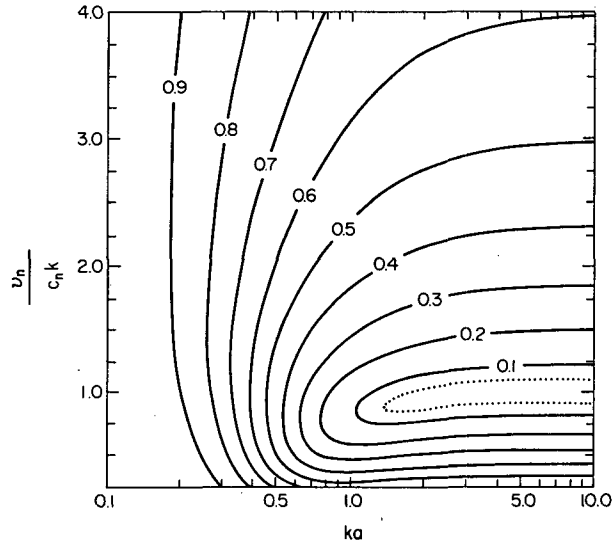

FIG. 5. Isopleths of $|R|$ as a function of ka and ν_n/c_nk for boundary condition II. The reflectivity of boundary condition I is a function of ka only and can be obtained by moving along the $\nu_n/c_nk = 1$ line in this figure.

[6]We note that the reflectivity of the boundary condition for balanced flow [either (5.4) or (5.8)] can be found in a similar fashion. The result is unit reflectivity. This suggests that the use of such a boundary condition in a primitive equation model would be a poor choice.

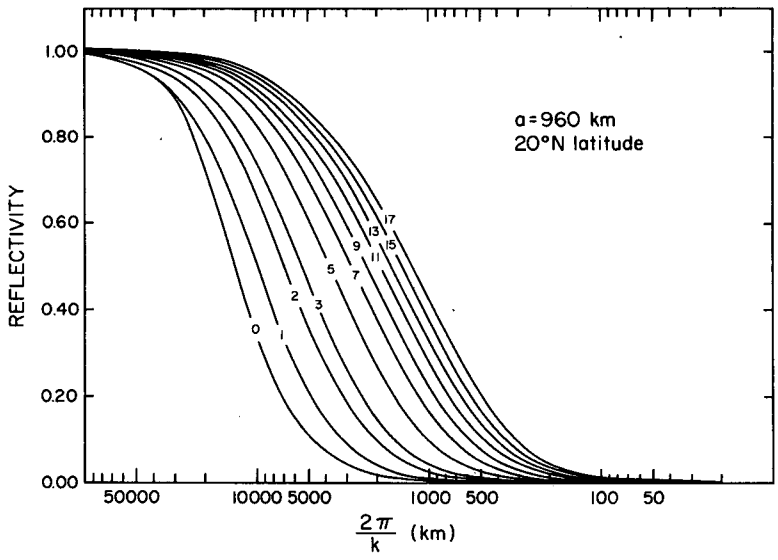

FIG. 6. The reflectivities of boundary condition II for the 18 vertical modes which have the eigenvalues listed in the last column of Table 1. These reflectivities have been calculated for a domain size of 960 km and for an f corresponding to a latitude of 20°N. The reflectivity of boundary condition I is essentially the same as the $n = 0$ curve.

from the $n = 0$ curve in Fig. 6. Even though boundary condition II does have higher reflectivities than I, for low-order vertical modes and horizontal wavelengths smaller than the size of the computational domain, the approximation made in boundary condition II does not introduce serious reflection problems.

6. Numerical examples

a. Single vertical mode

In this subsection we shall compare the results of numerical integrations of (2.20)–(2.22) using boundary conditions II, IV and V. In addition we shall show results obtained using the numerical extrapolation technique of Orlanski (1976). In Orlanski's method the condition

$$\frac{\partial u_n}{\partial t} + c_n \frac{\partial u_n}{\partial r} = 0 \qquad \text{(VIa)}$$

is used to predict u_n at the model boundary after

$$c_n = -\frac{\dfrac{\partial u_n}{\partial t}}{\dfrac{\partial u_n}{\partial r}}, \qquad \text{(VIb)}$$

has been used to diagnose c_n at the previous time step just inside the model boundary. The estimate of c_n is not allowed to become negative nor to exceed the radial grid interval divided by the time step. For further details the reader is referred to Orlanski's (1976) paper.

In order to conduct the following single mode tests we have made use of the numerical model described in the Appendix. In the experiments illustrated here, the fluid is initially at rest but has a free surface perturbation

$$\Phi_n(r,0) \propto \left\{ \frac{r^2}{2r_0^2}\left[1 + \frac{4 - r^2/r_0^2}{4 + f^2 r_0^2/c_n^2}\right] - 1 \right\} \exp(-r^2/2r_0^2), \qquad (6.1)$$

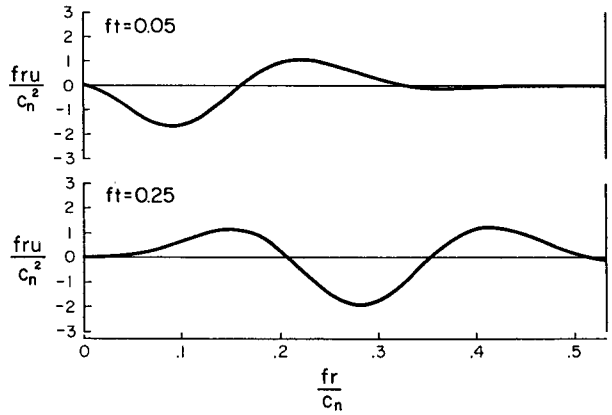

FIG. 7. The fru/c_n^2 field at $ft = 0.05$ and 0.25 for all single vertical mode initial value experiments. See text for further discussion.

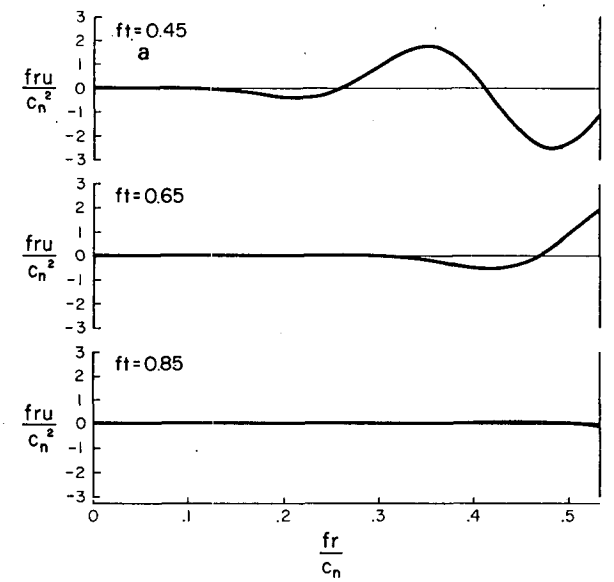

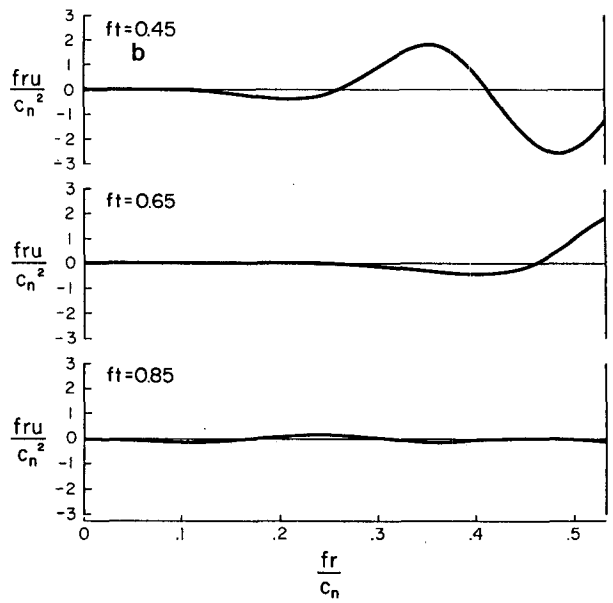

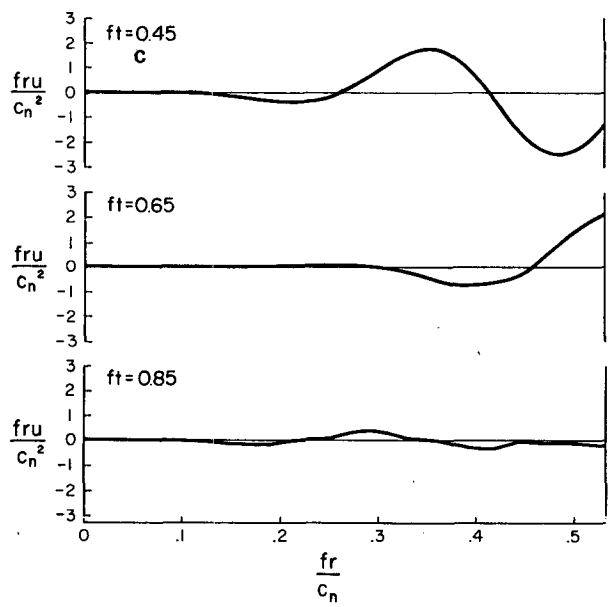

FIG. 8. The fru/c_n^2 field at $ft = 0.45$, 0.65 and 0.85 for single vertical mode initial value experiments employing (a) infinite domain, (b) boundary condition II, (c) boundary condition VI, (d) boundary condition IV and (e) boundary condition V.

where r_0 is a measure of the perturbation half width which has been specified to be $r_0 = 0.1c_n/f$. This initial value problem was first studied by Obukhov (1949). For the linear problem, the final geostrophically adjusted state can be obtained analytically by solving the potential vorticity equation (Schubert *et al.*, 1980, Section 6), providing an independent check on the performance of the model.

The results of five experiments will now be shown, the first being the control or "infinite domain" experiment and the remaining four using boundary conditions II, IV, V and VI. In the infinite domain experiment the computational domain was expanded to eliminate all possible boundary effects on the solution in the interior ($fr/c_n \leq 0.5375$) of the model. The results of the five numerical tests are shown in Figs. 7 and 8. Fig. 7 is common to all those given in Fig. 8, and shows the early propagation of the wave which is excited in the u field (the divergent component of the wind). Up to time $ft = 0.25$, the numerical solutions are essentially the same for all five experiments. After this time, how-

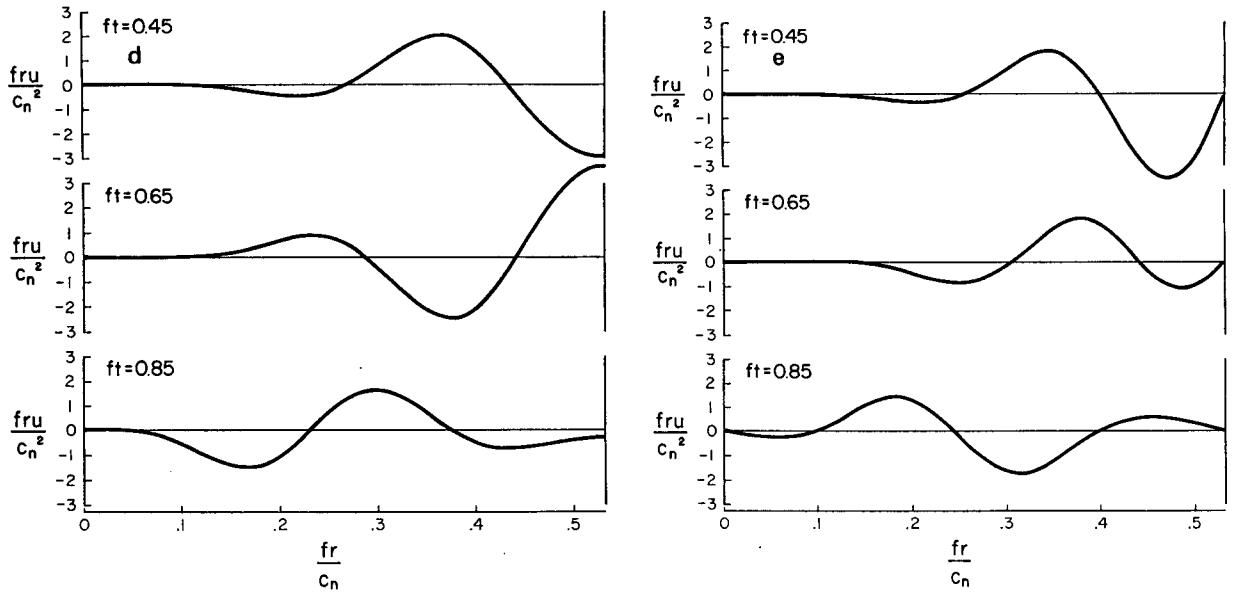

FIG. 8. (*Continued*)

ever, the solutions diverge due to the differences in the lateral boundary conditions, as can be seen in Fig. 8. Fig. 8a shows the results of the control experiment and can be regarded as the ideal result since there are no boundary effects. We see that at $ft = 0.85$, the computational domain is for the most part in geostrophic balance. In the interior, $fr/c_n \leq 0.5$, the solution is well within 1% of the analytically calculated final adjusted state. The remaining figures show the numerical solutions for those experiments incorporating boundary condition II (Fig. 8b), boundary condition VI (Fig. 8c), boundary condition IV (Fig. 8d) and boundary condition V (Fig. 8e). Note that although boundary conditions IV and V both have theoretical reflectivities of one, the wave which is excited in the radial wind field is not reflected in an identical manner, i.e., a phase shift occurs when using boundary condition IV, the condition of zero divergence. This is a consequence of forcing the radial wind at the boundary to be proportional to its horizontal derivative rather than to a constant as is done in the case of zero mass flux. Such a phase shift should not be misinterpreted as a difference in the reflectivities of boundary conditions IV and V. Clearly, boundary conditions II and VI give considerably better results with boundary condition II most closely approximating the control experiment.

b. Fully stratified case

We extend the results of Section 6a by comparing the behavior of boundary conditions II, IV, V and VI in a stratified numerical model and by considering an additional boundary condition for which the relation

$$\frac{\partial u}{\partial t} + c\,\frac{\partial u}{\partial r} = 0 \qquad \text{(VII)}$$

is applied at the lateral boundary grid points where the phase velocity c is a constant chosen to be representative of the first internal mode of the model (Klemp and Wilhelmson, 1978).

An 18-level axisymmetric primitive equation model is used to conduct these numerical tests. The system (2.2)–(2.7) is solved where the time and horizontal space differencing are the same as those used in the divergent barotropic model described in the Appendix. Vertical differencing follows the scheme developed for the UCLA GCM (Arakawa and Lamb, 1977), where $p_T = 100$ mb. The computational domain of 960 km consists of 64 grid intervals ($I = 65$).

Boundary conditions IV, V, VI and VII are all applied level by level. However, in order to apply boundary condition II it is necessary to project the boundary values of the dependent variables onto the vertical structure functions and thus obtain the amplitude of each vertical mode. In practice, we obtain these vertical structure functions via a method which will more accurately represent the effects of the vertical differencing scheme we have employed. This approach can be summarized as follows. Noting that boundary condition II is asymptotically valid as $k \to \infty$, and that in this case f can be elim-

inated,[7] we can linearize (2.2)–(2.7), assume a solution of the form

$$\begin{Bmatrix} u(r,\sigma,t) \\ T(r,\sigma,t) \\ \pi(r,t) \end{Bmatrix} = \begin{Bmatrix} \hat{u}(\sigma)[H_1^{(1)}(kr) + RH_1^{(2)}(kr)] \\ \hat{T}(\sigma)[H_0^{(1)}(kr) + RH_0^{(2)}(kr)] \\ \hat{\pi}[H_0^{(1)}(kr) + RH_0^{(2)}(kr)] \end{Bmatrix} e^{-i\nu t}, \quad (6.2)$$

and obtain

$$i\frac{\nu}{k}\hat{u} + \int_\sigma^1 \overline{\pi}\,\overline{\alpha}\left(\frac{\hat{T}}{\overline{T}} + \frac{p_T}{\overline{p}}\frac{\hat{\pi}}{\overline{\pi}}\right) d\sigma' + \sigma\,\overline{\alpha}\,\hat{\pi} = 0, \quad (6.3)$$

$$i\frac{\nu}{k}\hat{T} - \frac{d\overline{T}}{d\sigma}\sigma\int_0^1 \hat{u}\,d\sigma + \left(\frac{d\overline{T}}{d\sigma} - \frac{\overline{\pi}\,\overline{\alpha}}{c_p}\right)\int_0^\sigma \hat{u}\,d\sigma' = 0, \quad (6.4)$$

$$i\frac{\nu}{k}\hat{\pi} - \overline{\pi}\int_0^1 \hat{u}\,d\sigma = 0. \quad (6.5)$$

In practice, we follow the above procedure with the governing equations in differential-difference form (radius and time being continuous, sigma discrete).[8] Then the above integrals become sums and we can regard the resulting problem as an algebraic eigenvalue problem, with ν/k as the eigenvalue. For a vertically discrete model atmosphere with N velocity levels (6.3)–(6.5) yields a system of either $2N$ or $2N + 1$ vertically discrete equations depending on whether the temperature levels are staggered. For Lorenz (1960) type vertical differencing schemes (nonstaggered temperature) there are $2N + 1$ vertically discrete equations. This allows the mass field one additional degree of freedom which is not under the control of the geostrophic adjustment process. Although the results presented here are from a model with Lorenz type vertical differencing, the extra degree of freedom in the mass field does not seem to present any problems. The eigenvectors obtained from the solution of the discrete versions of (6.3)–(6.5) are not orthogonal, but this poses no difficulty with respect to the projection process since it is easy to calculate from the transpose of the coefficient matrix a set of eigenvectors which are orthogonal to the original set (e.g., Twomey, 1977, Chap. 4).

For a numerical experiment we again consider an initial value problem in which a Gaussian perturbation is introduced in the π or surface pressure field. Thus, the initial π field is of the form

$$\pi(r,0) = \overline{\pi} - A\exp[-(r/r_0)^2], \quad (6.6)$$

where $r_0 = 150$ km, $A = 1$ mb and $\overline{\pi}$ is a specified constant. The initial temperature field is independent of radius along constant σ surfaces and the initial motion field is identically zero.

A control experiment is first conducted for which the lateral boundary is moved to 3840 km in order to exclude boundary effects on the numerical solution in the interior 960 km. The vertical motion field at $t = 6$ h is displayed for all the experiments in Fig. 9. Fig. 9a, which corresponds to the control or infinite domain experiment, is the desired result, and indicates that only relatively small amplitude (high vertical wavenumber) motions remain in the computational domain at this time. Boundary conditions II and VI (Figs. 9b and 9c) appear to give results closest to the control experiments with boundary conditions IV and V (Figs. 9f and 9e) deviating significantly from the control. Fig. 10 illustrates the reflected vertical motion field for boundary conditions VII, V and IV where the contour intervals are 2.5 mb day^{-1}. Since the reflections for boundary conditions II and VI are much smaller, they are given separately in Fig. 11 where the contour interval is reduced by a factor of 10 to 0.25 mb day^{-1}. For the cases of zero radial wind (Fig. 10b) and zero divergence (Fig. 10c) we see that the external mode and first internal mode have reached the boundary and have been reflected.[9] Boundary condition VII gives much better results than either of these since the amplitude of the external mode is significantly reduced, and very little of the first internal mode is reflected. These results should be expected since the constant phase speed has been chosen to be representative of the first internal mode. The theoretical reflectivity for boundary condition VII can be calculated for each vertical mode and reveals that the choice of a single phase speed results in large reflectivities for all vertical modes except for those modes which propagate at a rate which is close to the chosen c. This result appears to be independent of the choice of c, suggesting a fundamental weakness in choosing a constant phase speed to represent all waves.

The reflected vertical motion fields shown in Fig. 11 indicate that boundary condition VI gives stronger reflection than does boundary condition II. In ad-

[7]For such a situation the following procedure does not address the boundary condition on the tangential wind component. Thus, we have arbitrarily chosen to apply the condition of zero vorticity, $\partial rv(r,t)/r\partial r = 0$.

[8]Details of this procedure can be found in Hack, J. J., and W. H. Schubert, 1980: The role of convective-scale processes in tropical cyclone development. Atmos. Sci. Pap. No. 330, Colorado State University.

[9]In fact, the external mode has been reflected three times, while the first internal mode has experienced only one reflection.

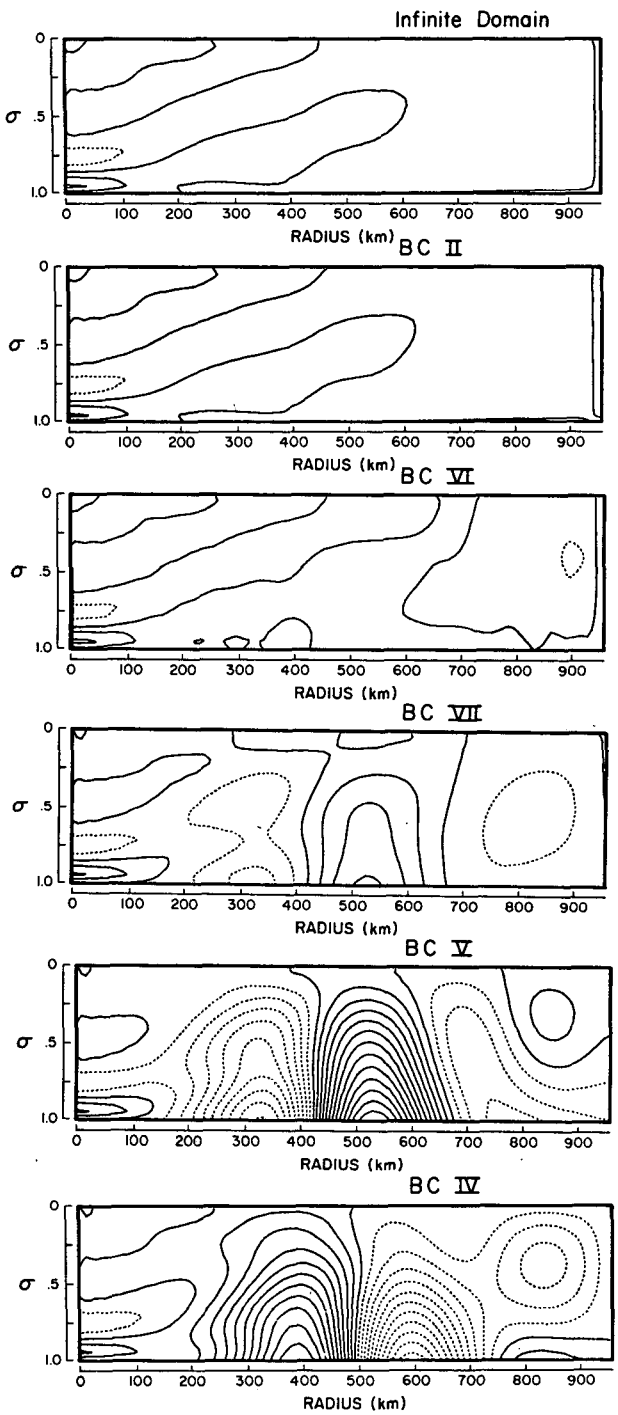

FIG. 9. The vertical motion field ω at $t = 6$ h for the fully stratified initial value experiments employing (a) infinite domain, (b) boundary condition II, (c) boundary condition VI, (d) boundary condition VII, (e) boundary condition V and (f) boundary condition IV. The contour interval is 2.5 mb day^{-1} with dashed lines indicating sinking motion.

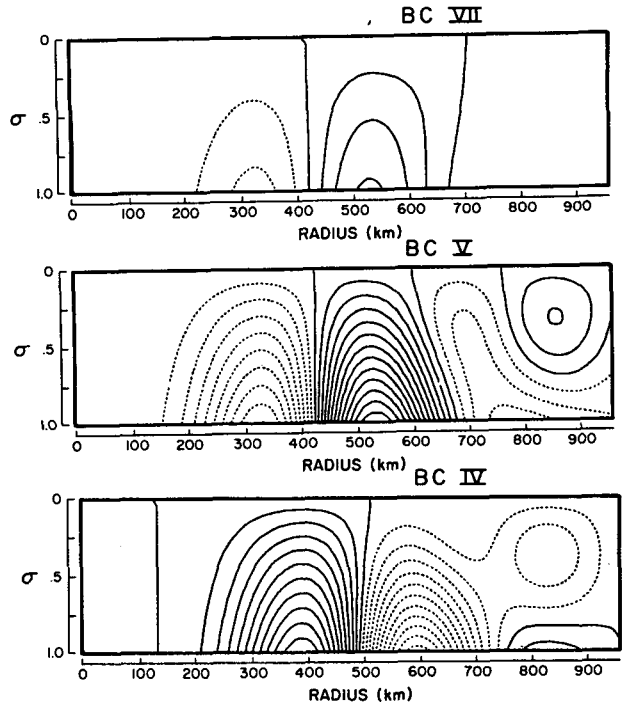

FIG. 10. The reflected vertical motion field at $t = 6$ h for the fully stratified initial value experiments employing (a) boundary condition VII, (b) boundary condition V and (c) boundary condition IV. The contour interval is 2.5 mb day^{-1} with dashed lines indicating sinking motion.

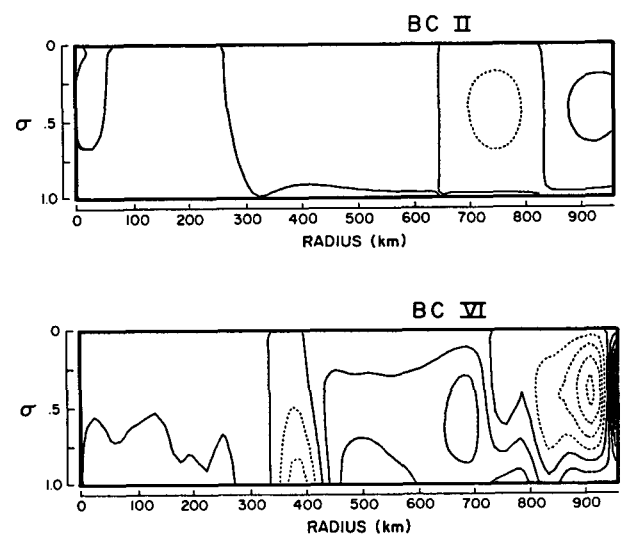

FIG. 11. The reflected vertical motion field at $t = 6$ h for the fully stratified initial value experiments employing (a) boundary condition II and (b) boundary condition VI. The contour interval is 0.25 mb day^{-1} with dashed lines indicating sinking motion.

dition, a considerable amount of computational noise has been introduced into the reflected waves by boundary condition VI. One other interesting aspect associated only with boundary condition VI is the appearance of a fictitious mass sink for the computational domain, a mass trend which could have an adverse impact on long-term numerical integrations.

7. Concluding remarks

In a tropical cyclone any balance which may exist between the mass and wind fields is continually disrupted by the release of latent heat in deep cumulus convection. In response, the atmosphere continually tries to adjust back to a balanced state and in the process radiates gravity-inertia waves. The energy analysis of Section 4 suggests that, at times, a large fraction of the energy generated by the release of latent heat can be partitioned to gravity-inertia waves rather than to geostrophic flow. Thus it is important that a numerical model of a tropical cyclone employ an appropriately formulated lateral boundary condition, i.e., one which does not reflect outward propagating gravity-inertia waves.

We have demonstrated that it is possible to derive approximate outgoing wave conditions (boundary conditions I–III) for the fully stratified axisymmetric case. We have examined theoretically the reflectivities of these three approximate conditions as well as two other lateral boundary conditions in common use, the conditions of zero divergence and zero radial wind (boundary conditions IV and V). The results of this analysis show that boundary condition I has the lowest reflectivity, although boundary condition II, which is much easier to implement, is nearly as good for the lower order vertical modes. We are presently using II in an axisymmetric tropical cyclone model. It is also clear from our analysis that the condition of zero divergence is not in the true sense an "open" lateral boundary condition since it results in unit reflection of gravity-inertia waves. In this regard, it is as poor a boundary condition as the condition of zero radial wind, which also gives unit reflection.

The behavior of two other lateral boundary conditions has been examined numerically. These are the method proposed by Orlanski (1976) (boundary condition VI) and the method proposed by Klemp and Wilhelmson (1978) (boundary condition VII). The basic problem with the latter approach in tropical cyclone models is the choice of a single phase speed to represent all waves. Only those waves moving at or very near this phase speed will be treated properly, and since there is such a wide range of propagation speeds in a stratified model, it is difficult to tune the choice of this constant phase velocity. However, in the situation where an external mode does not occur, or where the amplitude spectrum of the vertical modes which are excited in the model has a narrow distribution, boundary condition VII may give fairly good results.

Although there is some reflection (5–15%) associated with boundary condition VI, it produces results which at first glance appear to closely approximate those of the control experiment. We believe, however, that there are several problems associated with boundary condition VI. Since this method is applied level by level it may have difficulty when two or more vertical modes (moving at different phase velocities) reach the boundary simultaneously. This vertically independent specification of the lateral boundary condition in a hydrostatic model is questionable from a theoretical viewpoint since the results of Sections 2 and 5 suggest that the boundary condition should be applied to each vertical mode. For the examples we have examined, the numerical estimates of the phase velocity c tend to vary considerably, which apparently introduces noise into the computational domain. In addition we have experienced fictitious mass trends when using boundary condition VI.

Although boundary condition II has been shown to give reasonably good results in the fully stratified case, it is by no means perfect. It includes both the asymptotic approximation for Hankel functions and the pure gravity wave approximation for the gravity-inertia wave frequency. Numerical initial value experiments, which are similar to those conducted in Section 6b, but which include a balanced basic-state flow, show that the balanced flow is not improperly altered when using boundary condition II, even after gravity wave activity has left the computational domain.

Somewhat better results could undoubtedly be obtained by using boundary condition I, but this involves a knowledge of the spectral characteristics of the outgoing waves. It is not obvious that such a slight improvement in results would justify the additional effort.

Acknowledgments. The authors are grateful to Duane Stevens, Scott Fulton, Yoshio Kurihara, David Williamson and Roger Daley for their valuable comments on this work. We are also indebted to Odilia Panella for her help in preparing the manuscript. The research reported here has been supported by the National Science Foundation (Grants ATM-7808125 and ATM-8009799) and the Office of Naval Research (Grant N00014-79-C-0793). Acknowledgment is also made to the National Center for Atmospheric Research, which is sponsored by the National Science Foundation, for computer time used in this research.

APPENDIX

Finite-Difference Form of the Divergent Barotropic System of Equations

The nonlinear divergent barotropic system of equations can be written in flux form as

$$\frac{\partial}{\partial t}(\phi r u) + \frac{\partial}{\partial r}(\phi r u u) - \left(f + \frac{v}{r}\right)\phi r v + \phi r \frac{\partial \phi}{\partial r} = 0, \quad \text{(A1)}$$

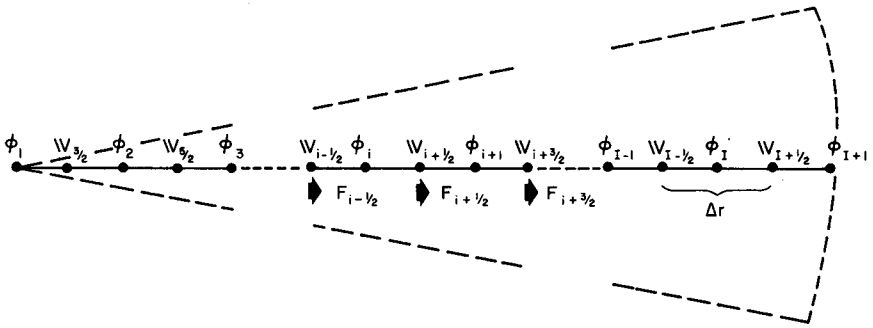

FIG. A1. Schematic of the horizontal finite-differencing scheme.

$$\frac{\partial}{\partial t}(\phi r v) + \frac{\partial}{\partial r}(\phi r u v) + \left(f + \frac{v}{r}\right)\phi r u = 0, \quad \text{(A2)}$$

$$\frac{\partial \phi r}{\partial t} + \frac{\partial \phi r u}{\partial r} = 0, \quad \text{(A3)}$$

where the dependent variables u, v (the radial and tangential velocity components) and ϕ (the free surface geopotential) are functions of (r,t) only. Using the staggered finite-difference grid shown in Fig. A1 (scheme B, Arakawa and Lamb, 1977), Eqs. (A1)–(A3) may be written in a differential difference form as

$$\frac{\partial \Phi_i}{\partial t} = -(F_{i+1/2} - F_{i-1/2}), \quad \text{(A4)}$$

$$\begin{aligned}\frac{\partial}{\partial t}(\Phi_{i+1/2}u_{i+1/2}) = {} & -\tfrac{1}{2}[\mathscr{F}_{i+1}(u_{i+1/2} + u_{i+3/2}) \\ & - \mathscr{F}_i(u_{i-1/2} + u_{i+1/2})] + \tfrac{1}{4}[(\phi_i \\ & + \phi_{i+1})(C_i + C_{i+1})]\, v_{i+1/2} - \tfrac{1}{2}r_{i+1/2}(\phi_i \\ & + \phi_{i+1})(\phi_{i+1} - \phi_i),\end{aligned} \quad \text{(A5)}$$

$$\begin{aligned}\frac{\partial}{\partial t}(\Phi_{i+1/2}v_{i+1/2}) = {} & -\tfrac{1}{2}[\mathscr{F}_{i+1}(v_{i+1/2} + v_{i+3/2}) \\ & - \mathscr{F}_i(u_{i-1/2} + u_{i+1/2})] - \tfrac{1}{4}[(\phi_i \\ & + \phi_{i+1})(C_i + C_{i+1})]\, u_{i+1/2},\end{aligned} \quad \text{(A6)}$$

where

$$\begin{aligned}\Phi_i &\equiv \phi_i r_i \Delta r \\ F_{i+1/2} &\equiv \tfrac{1}{2}(\phi_i + \phi_{i+1})\, r_{i+1/2}\, u_{i+1/2} \\ \Phi_{i+1/2} &\equiv \tfrac{1}{2}(\Phi_i + \Phi_{i+1}) \\ \mathscr{F}_i &\equiv \tfrac{1}{2}(F_{i-1/2} + F_{i+1/2}) \\ C_i &\equiv f r_i\, \Delta r + \tfrac{1}{2}(v_{i-1/2} + v_{i+1/2})\, \Delta r\end{aligned} \quad \text{(A7)}$$

The model used to produce the results presented in Section 6a consists of 43 velocity points and 44 geopotential points ($I = 43$) spaced 0.0125 dimensionless units apart [i.e., $\Delta r = 0.0125(gh)^{1/2}/f$]. Time differencing of (A4)–(A6) is accomplished with a leapfrog scheme coupled with an Asselin (1972) time filter.

For the linear initial value problems discussed in Section 6a, we have applied the lateral boundary condition to all predicted variables [i.e., the tendencies $u_{I+1/2}$, $v_{I+1/2}$ and ϕ_{I+1} are predicted by the lateral boundary condition while all other tendencies are evaluated using (A4)–(A6)]. Horizontal derivatives at the boundary points are computed using a first order one-sided difference.

REFERENCES

Anthes, R. A., 1971: A numerical model of the slowly varying tropical cyclone in isentropic coordinates. *Mon. Wea. Rev.*, **99**, 617–635.

——, 1972: Development of asymmetries in a three-dimensional numerical model of the tropical cyclone. *Mon. Wea. Rev.*, **100**, 461–476.

——, 1977: Hurricane model experiments with a new cumulus parameterization scheme. *Mon. Wea. Rev.*, **105**, 287–300.

——, S. L. Rosenthal and J. W. Trout, 1971a: Preliminary results from an asymmetric model of the tropical cyclone. *Mon. Wea. Rev.*, **99**, 744–758.

——, J. W. Trout and S. L. Rosenthal, 1971b: Comparisons of tropical cyclone simulations with and without the assumption of circular symmetry. *Mon. Wea. Rev.*, **99**, 759–766.

Arakawa, A., and V. R. Lamb, 1977: Computational design of the basic dynamical processes of the UCLA general circulation model. *Meth. Comput. Phys.*, **17**, 173–265.

Asselin, R., 1972: Frequency filter for time integrations. *Mon. Wea. Rev.*, **100**, 487–490.

Bennett, J. R., 1976: Open boundary conditions for dispersive waves. *J. Atmos. Sci.*, **33**, 176–182.

Daley, R., 1979: The application of non-linear normal mode initialization to an operational forecast model. *Atmos.-Ocean*, **17**, 97–124.

Elvius, T., 1977: Experiments with a primitive equations model for limited area forecasts. *Beitr. Phys. Atmos.*, **50**, 367–392.

Gray, W. M., E. Ruprecht and R. Phelps, 1975: Relative humidity in tropical weather systems. *Mon. Wea. Rev.*, **103**, 685–690.

Harrison, E. J., 1973: Three-dimensional numerical simulations of tropical systems utilizing nested finite grids. *J. Atmos. Sci.*, **30**, 1528–1543.

Jones, R. W., 1977: A nested grid for a three-dimensional model of a tropical cyclone. *J. Atmos. Sci.*, **34**, 1528–1553.

Kasahara, A., and K. Puri, 1981: Spectral representation of three-dimensional global data by expansion in normal mode functions. *Mon. Wea. Rev.*, **109**, 37–51.

Klemp, J. B., and R. B. Wilhelmson, 1978: The simulation of three-dimensional convective storm dynamics. *J. Atmos. Sci.*, **35**, 1070–1096.

Kuo, H. L., 1965: On formation and intensification of tropical cyclones through latent heat release by cumulus convection. *J. Atmos. Sci.*, **22**, 40–63.

Kurihara, Y., 1975: Budget analysis of a tropical cyclone simulated in an axisymmetric numerical model. *J. Atmos. Sci.*, **32**, 25–59.

——, and R. E. Tuleya, 1974: Structure of a tropical cyclone developed in a three-dimensional numerical simulation model. *J. Atmos. Sci.*, **31**, 893–919.

——, G. J. Tripoli and M. A. Bender, 1979: Design of a moveable nested-mesh primitive equation model. *Mon. Wea. Rev.*, **107**, 239–249.

Lorenz, E. N., 1960: Energy and numerical weather prediction. *Tellus*, **12**, 364–373.

Madala, R. V., and S. A. Piacsek, 1975: Numerical simulation of asymmetric hurricanes on a β-plane with vertical shear. *Tellus*, **27**, 453–468.

Mathur, M. B., 1974: A multi-grid primitive equation model to simulate the development of an asymmetric hurricane (Isebell, 1964). *J. Atmos. Sci.*, **31**, 371–393.

Obukhov, A. M., 1949: On the question of the geostrophic wind (in Russian). *Izv. Akad. Nauk SSSR Ser. Geograf. Geofiz.*, **13**, 281–306. [English transl. available from W. Schubert, Dept. Atmos. Sci., Colorado State University.]

Ogura, Y., 1964: Frictionally controlled, thermally driven circulation in a circular vortex with application to tropical cyclones. *J. Atmos. Sci.*, **21**, 610–621.

Ooyama, K., 1969a: Numerical simulation of the life cycle of tropical cyclones. *J. Atmos. Sci.*, **26**, 3–40.

——, 1969b: Numerical simulation of tropical cyclones with an axisymmetric model. *Proceedings of the WMO/IUGG Symposium on Numerical Weather Prediction*, Tokyo, III:81–88.

Orlanski, I., 1976: A simple boundary condition for unbounded hyperbolic flows. *J. Comput. Phys.*, **21**, 251–269.

Phillips, N. A., 1957: A coordinate system having some special advantages for numerical forecasting. *J. Meteor.*, **14**, 184–185.

Robert, A. J., J. Henderson and C. Turnbill, 1972: An implicit time integration scheme for baroclinic models of the atmosphere. *Mon. Wea. Rev.*, **100**, 329–335.

Rosenthal, S. L., 1970: A circularly symmetric primitive equation model of tropical cyclone development containing an explicit water vapor cycle. *Mon. Wea. Rev.*, **98**, 643–663.

——, 1971: The response of a tropical cyclone model to variations in boundary parameters, initial conditions, lateral boundary conditions, and domain size. *Mon. Wea. Rev.*, **99**, 767–777.

——, 1978: Numerical simulation of tropical cyclone development with latent heat release by the resolvable scales, I: model description and preliminary results. *J. Atmos. Sci.*, **35**, 258–271.

Schubert, W. H., J. J. Hack, P. L. SilvaDias and S. R. Fulton, 1980: Geostrophic adjustment in an axisymmetric vortex. *J. Atmos. Sci.*, **37**, 1464–1484.

Sundqvist, H., 1970a: Numerical simulation of the development of tropical cyclones with a ten-level model, part I. *Tellus*, **22**, 359–390.

——, 1970b: Numerical simulation of the development of tropical cyclones with a ten-level model, part II. *Tellus*, **22**, 504–510.

Twomey, S., 1977: *Introduction to the Mathematics of Inversion in Remote Sensing and Indirect Measurements*. Elsevier, 243 pp.

Yamasaki, M., 1968a: Numerical simulation of tropical cyclone development with the use of primitive equations. *J. Meteor. Soc. Japan*, **46**, 178–201.

——, 1968b: Detailed analysis of a tropical cyclone simulated with a 13-layer model. *Pap. Meteor. Geophys.*, **19**, 559–585.